

Spatial and temporal patterns of shoreline change of a 280-km high-energy disrupted sandy coast from 1950 to 2014: SW France



Bruno Castelle ^{a, b, *}, Benoit Guillot ^{a, b}, Vincent Marieu ^{a, b}, Eric Chaumillon ^c, Vincent Hanquiez ^{a, b}, Stéphane Bujan ^{a, b}, Coline Poppeschi ^{a, b}

^a CNRS, UMR EPOC, France

^b Univ. Bordeaux, UMR EPOC, France

^c Univ. La Rochelle, UMR CNRS LIENSs, France

ARTICLE INFO

Article history:

Received 24 August 2017

Received in revised form

16 October 2017

Accepted 8 November 2017

Available online 13 November 2017

Keywords:

Shoreline evolution

Tidal inlet

Coastal dunes

Coastal defence

Chronic erosion

ABSTRACT

A dataset of 15 geo-referenced orthomosaics photos was generated to address long-term shoreline change along approximately 270 km of high-energy sandy coast in SW France between 1950 and 2014. The coast consists of sandy beaches backed by coastal dunes, which are only disrupted by two wide tidal inlets (Arcachon and Maumusson), a wide estuary mouth (Gironde) and a few small wave-dominated inlets and coastal towns. A time and spatially averaged erosion trend of 1.12 m/year is found over 1950–2014, with a local maximum of approximately 11 m/year and a maximum local accretion of approximately 6 m/year, respectively. Maximum shoreline evolutions are observed along coasts adjacent to the inlets and to the estuary mouth, with erosion and accretion alternating over time on the timescale of decades. The two inlet-sandspit systems of Arcachon and Maumusson show a quasi-synchronous behaviour with the two updrift coasts accreting until the 1970s and subsequently eroding since then, which suggests that shoreline change at these locations is controlled by allocyclic mechanisms. Despite sea level rise and the well-established increase in winter wave height over the last decades, there is no capture of significant increase in mean erosion rate. This is hypothesized to be partly the result of relevant coastal dune management works from the 1960s to the 1980s after a long period of coastal dune disrepair during and after the Second World War. This study suggests that long-term shoreline change of high-energy sandy coasts disrupted by inlets and/or estuaries is complex and needs to consider a wide range of parameters including, non-extensively, waves, tides, inlet dynamics, sea level rise, coastal dune management and coastal defences, which challenges the development of reliable long-term coastal evolution numerical models.

© 2017 Elsevier Ltd. All rights reserved.

1. Introduction

The coastal zone is a major interface that is becoming increasingly topical and politically sensitive worldwide in a context of widespread erosion, increasing anthropogenic pressures (e.g. urban expansion, recreational development, Cohen, 1997; Ghermandi and Nunesn, 2013) and Climate Change (e.g. sea level rise, increase in storminess, Cazenave et al., 2014; Zappa et al., 2013). Coastal zones are increasingly exposed to erosion hazards, with eroding sectors often corresponding to sandy regions. Sandy coasts host recreational and leisure activities and provide outstanding ecosystem

values and services when comprising coastal dune systems (Martínez et al., 2013). Addressing the recent, say multi-decadal, shoreline change along sandy coasts is therefore of major interest for our understanding and modelling capability to predicting future evolutions.

Sandy coasts are amongst the most temporally and spatially variable coastal environments with their dynamic covering a wide range of temporal and spatial scales (Stive et al., 2002), from rapid storm-driven erosion (Masselink et al., 2016) to large-scale coastal change and shoreline translation as a result of sea level rise on geological timescales (Regnauld et al., 1996), through seasonal, interannual and multidecadal changes. While many studies focused on geological timescales, morphological change on the timescales from days to years have received substantial attention over the last decade as a result of increasingly building observational datasets

* Corresponding author. CNRS, UMR EPOC, France.

E-mail address: Bruno.castelle@u-bordeaux.fr (B. Castelle).

(Turner et al., 2016). Overall, these studies showed that the storm response and subsequent recovery of open sandy coasts are highly variable (Masselink et al., 2016; Scott et al., 2016), with erosion/recovery patterns cascading up through the scale to result in strong interannual variability sometimes exceeding in amplitude that of the seasonal variability (Robinet et al., 2016). These temporal patterns of shoreline change on open coasts are mostly controlled by the variability in incoming wave energy (Davidson et al., 2013; Splinter et al., 2014; Yates et al., 2009), while chronic changes are mostly governed by large-scale coastal sediment budget, including variation in river sediment supply, gradients in longshore sediment transport and sea level rise (Rosati, 2005; Pranzini and Williams, 2013).

The dynamics described above becomes increasingly blurred when approaching mixed energy environments, such as tidal inlets and estuary mouths, as these systems disrupt the longshore drift and sediment supply (Ridderinkhof et al., 2016). Such tidal systems typically exhibit cyclic and/or migrating behaviour. For instance, tidal inlets can migrate downdrift by hundreds of metres, resulting in erosion and accretion of the downdrift and updrift coast, respectively (Nienhuis et al., 2016). Along systems that are stable or quasi-stable alongshore, cyclic ebb-tidal delta dynamics from the timescales of months to years and decades (Cayocca, 2001; Ridderinkhof et al., 2016; Weidman and Ebert, 1993) is often observed as a result of the dominant longshore drift. This cyclic behaviour drives cyclic large-scale changes of the adjacent beaches, with erosion and accretion periods at the updrift and downdrift side alternating more or less out of phase over time (Castelle et al., 2007). Additional factors controlling shoreline change are the anthropogenic coastal works that have been performed over the last decades. These include, for instance, hard structures such as training walls to guide tidal inlets and groins that capture the longshore drift to locally nourish the updrift coast, or softer approaches such as beach nourishments (e.g. Grunnet and Ruessink, 2005), artificial sand bypassing and submerged breakwater (Ranasinghe and Turner, 2006; Bouvier et al., 2017). Hard structures can be effective in fixing the shoreline and in protecting the hinterland from marine flooding. However, they also most of the time cause adverse effects (Firth et al., 2014), for instance at the downdrift coast due to the disruption or sometimes the interruption of the longshore transport.

Sea level rise has long been assumed as the primary cause for the observed chronic shoreline erosion (e.g. Vellinga and Leatherman, 1989). Sea-level-rise driven shoreline erosion can be estimated through the Bruun rule and its variants (Bruun, 1962; Weggel, 1979) that assume that the nearshore profile translates upward and landward to adjust to sea level rise, which is referred to as Bruun effect. The Bruun rule showed poor agreement with observation in many locations worldwide (e.g. List et al., 1997), and was therefore strongly criticized (Cooper and Pilkey, 2004). However, one can argue that the disagreement was to some extent due to the omission of all the other forcing factors discussed above, and that the Bruun rule may provide a fair indication of the isolated impact of sea level rise. In a recent probabilistic study, Le Cozannet et al. (2016) showed that the impact of sea level rise on open coasts can only be captured on long (say > 50 years) timescales while other processes such as longshore sand transport and interannual wave energy variability control shoreline evolution on shorter timescales. Ranasinghe et al. (2013) showed that sea-level-rise driven shoreline change adjacent to commonly found tidal inlets is not only influenced by the Bruun effect, but also mostly by sea-level-rise driven basin infilling, and potentially other factors such as Climate-Change driven variations in rainfall/runoff.

Shoreline changes can be measured through various means. Over the last 2 decades, an array of survey methods (e.g. DGPS,

Lidar, video monitoring) have been used to build relevant morphological datasets (Turner et al., 2016). These methods are, however, limited in time (e.g. Lidar) or space (e.g. DGPS) and cannot provide large-scale and long-term (>50 years, > 10 km) shoreline evolution. Instead, remote sensing of the Earth through satellite images can provide large-scale shoreline change information (Almonacid-Caballer et al., 2016; Ford, 2013). Complementary, the analysis of historical aerial photographs can provide additional data prior to the deployment of the satellites providing high-resolution images (Chaaban et al., 2012). Overall, combining satellite images and historical photographs, and historical charts when available, is the only method enabling a quantitative assessment of shoreline change on large temporal (>50 years) and spatial (>10 km) scales.

In this paper, 270 km of the high-energy sandy coast of SW France is addressed using a diachronic analysis of georeferenced aerial photographs since 1950. The study site is described in Section 2 before giving the material and methods in Section 3. Results are presented in Section 4 and further discussed in Section 5 before conclusions are drawn in Section 6.

2. Study area

The study area is located in SW France and covers approximately 270 km of sandy beaches (Fig. 1). It extends from the south of Oléron Island in the north to the mouth of the Adour River in the south. The studied area is mostly a sedimentary coastline, at the exception of the northern (Fig. 1) and southern part of the Gironde Estuary where rocky basement locally outcrops (Chaumillon et al., 2008). This sedimentary shoreline is bounded by rocky shorelines to the north (northern part of the Oléron Island, Chaumillon et al., 2008). This 270 km-long stretch of sandy beaches is disrupted by two wide inlets (Maumusson and Arcachon inlets, Fig. 1) and one large estuary mouth (Gironde estuary, Fig. 1), all corresponding to incised-valley segments (Chaumillon et al., 2008; Féliès et al., 2010). Those incised valley segments display an overall northwest southeast orientation, controlled by faults and alternation of hard and soft strata (Allard et al., 2010; Chaumillon et al., 2008; Féliès et al., 2010; Klingebiel and Gayet, 1995). This northwest southeast trend is inherited from the Hercynian faults, reactivated during the opening of the Bay of Biscay and the Pyrenean collision (Chaumillon et al., 2008). Based on the location of incised-valleys and associated inlets and estuaries disrupting the coastline, four distinct coastal compartments can be distinguished: (1) The northern compartment corresponds to the southern sector of the Oléron Island that comprises approximately 15 km of relatively straight W-WSW facing open beaches that are delimited by the rocky part of the Oléron Island to the north and by the Maumusson inlet (Fig. 1b) in the south where the coast forms a sandspit (Gatseau spit); (2) The Arvert peninsula comprises approximately 15 km of W-facing straight beaches, and is delimited by the Maumusson inlet to the north and by the Bonne Anse lagoon-inlet system and the mouth of the Gironde estuary to the south (Fig. 1c); (3) The Gironde coast, which is characterized by a 110-km stretch of open sandy beaches dominantly facing W-WNW, although with more variability in the northern sector. This sector is characterized by the presence of reasonably small coastal towns with limited coastal defences, e.g. Soulac and Lacanau. This compartment is delimited by the Cap Ferret sandspit at the mouth of the Arcachon Lagoon to the south (Fig. 1d); (4) The Landes coast extends approximately 120 km and comprises W-WNW facing sandy beaches that are only disrupted by the small-scale wave-dominated inlets of Mimizan, Contis-les-Bains, Capbreton and Huchet, with only the latter being not trained by jetties (Fig. 1d). Further south of Huchet inlet, the coastal town of Capbreton is also protected by various coastal structures (jetties and groins). Of note, Capbreton also faces the Capbreton

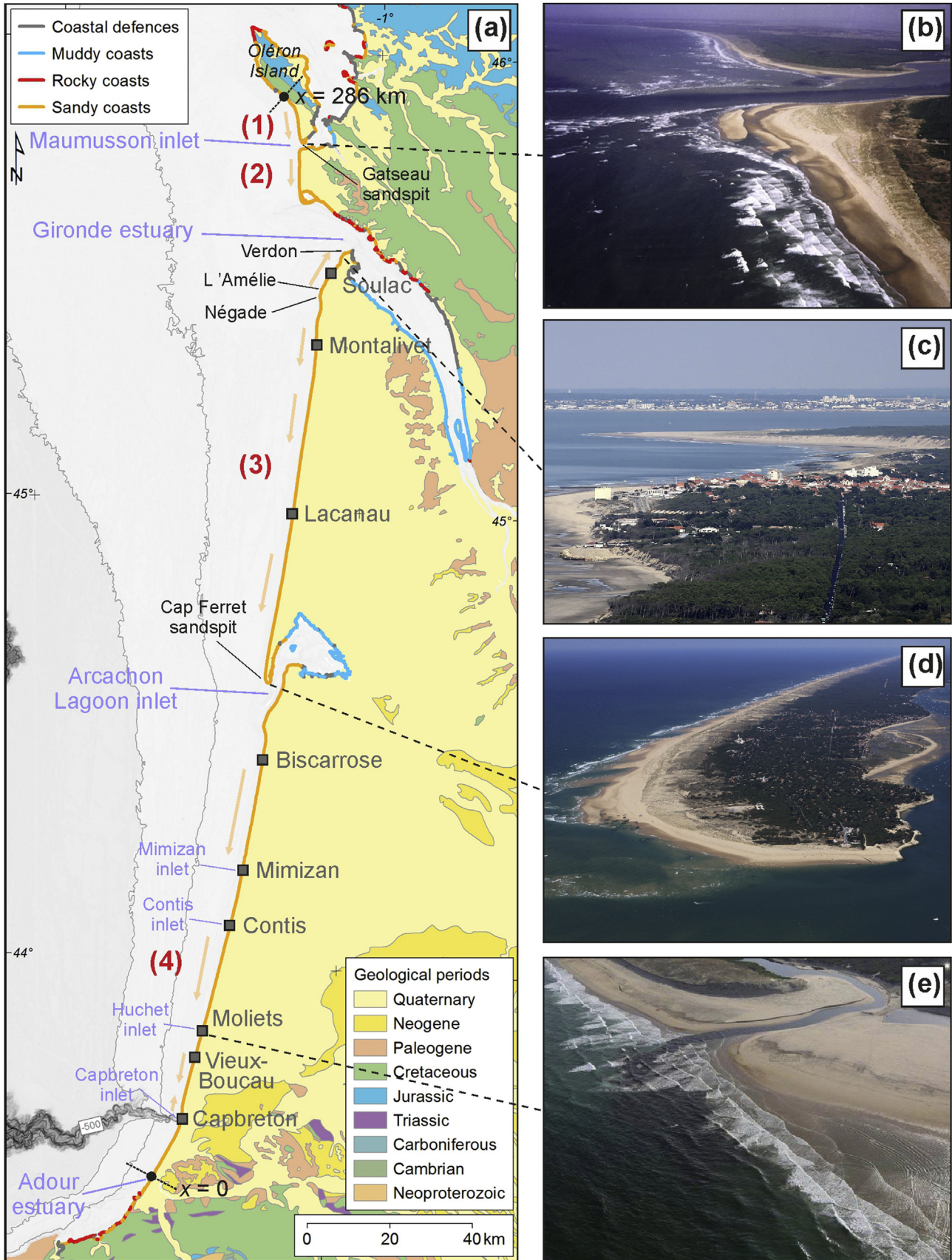


Fig. 1. Study area between $x = 0$ and $x = 286$ km essentially composed of sandy coasts with indication of the inherited geology. Note that rocks can locally outcrop in the intertidal and subtidal domain at some of the sandy beaches in the northern sector of Oléron and in south of the Gironde estuary (Chaumillon et al., 2008; Feniès et al., 2010). The grey squares indicate the location of the small coastal towns with their seafront more or less built on the coastal dunes. Four coastal compartments are distinguished with from north to south: (1) south Oléron coast; (2) Arvert peninsula; (3) Gironde coast; (4) Landes coast. The sandy arrows indicate the direction and magnitude of the net longshore drift. Aerial photographs of some relevant coastal forms: (b) the Maumusson inlet; (c) the coastal town of Soulac with the Gironde estuary in the background (Ph. J. Augereau, @Lacanau Council); (d) the Cap Ferret sandspit (@Observatoire de la Côte Aquitaine); (e) the wave-dominated Huchet inlet (Ph. I. Louvier).

Canyon (Fig. 1) that deeply affects incoming waves and, in turn, the nearshore currents and sediment pathways in this area (Mazieres et al., 2014). The Landes coast is delimited by the Adour river



Fig. 2. Aerial photographs of (a) the typical landscape of the study area with sandy beaches backed by high and wide coastal dunes, (b) the coastal town of Lacanau with its seafront built on the dune, a similar setting to e.g. Montalivet and Mimizan and (c) localized areas under severe chronic erosion with the loss of the coastal dune exposing the coastal forest to marine erosion. Photographs (a,b) by J. Augereau (@Lacanau Council) and (c) by B. Castelle.

mouth in the south, with the northern seawall extending approximately 900 m offshore. All the sandy beaches of these 4 sectors are backed by high and wide coastal dunes (Fig. 2a), except along some of the coastal towns (Capbreton, Mimizan, Biscarrosse, Montalivet, Soulac and Lacanau see Fig. 2b) and in areas under severe chronic erosion where the coastal dune was completely eroded leaving the coastal forest exposed to ocean waves (e.g. Gatseau, Baumann et al., 2017; and Pointe de la Négade, see Fig. 2c).

Beaches are primarily composed of fine to medium quartz sand, although coarser sand (e.g. in the south of the Landes coast) and even pebbles can be found locally. The coast is meso-macrotidal with the tidal range increasing from south to north owing to the widening continental shelf (Le Cann, 1990). Neap tidal range is typically smaller than 1.5 m with the highest astronomical tidal range ranging from approximately 5 m in the south to 6.5 m in the north of the study area. The most frequent and strongest wind events are from the WSW and NNW. The wave climate is energetic with a dominant W to NW incidence and a strong seasonal variability (Butel et al., 2002). For instance, the monthly-averaged significant wave height along the Gironde coast in the middle of the study area ranges from 1.11 m in July with a dominant W-NW direction to 2.4 m in January with dominant W direction (Castelle et al., 2017a). Incoming winter waves show a strong interannual variability, owing to natural modes of climate variability, primarily the West Europe Pressure Anomaly (Castelle et al., 2017b) and to a lesser extent the North Atlantic Oscillation (Dodet et al., 2010). Offshore significant wave height at the open beaches can exceed 8 m during severe storms (Castelle et al., 2015; Baumann et al., 2017). Overall, the wave height slightly increases southwards because of the narrowing continental shelf reducing the bottom friction and resulting in less energy dissipation of the incoming ocean waves. The dominant W-NW wave climate drives a net southerly longshore drift (Bertin et al., 2008; Idier et al., 2013), except in localized NW-facing sectors (e.g. Soulac) where the longshore drift reverses. The southerly longshore drift varies considerably (Fig. 1) with, from north to south, approximately $100.10^3 \text{ m}^3/\text{year}$ at the south Oléron coast and Avert Peninsula (Bertin et al., 2008); $100.10^3\text{--}350.10^3 \text{ m}^3/\text{year}$ along the Gironde coast (Idier et al., 2013) and $350.10^3\text{--}600.10^3 \text{ m}^3/\text{year}$ along most of the Landes coast. Within the latter sector, the longshore drift locally reverses north of Capbreton owing to the Capbreton canyon (Abadie et al., 2006; Mazieres et al., 2014) and becomes negligible between Capbreton and the Adour estuary owing to the dominant shore-normal wave incidence (Abadie et al., 2006).

3. Materials and methods

3.1. Aerial photographs

Aerial photographs of the SW coast of France were gathered from the French National Institute of Geographic and Forest Information (IGN). From 1950 to 2014, 15 series of aerial photographs covering partly or entirely the study area were collected and further analysed (see Table 1 for the main survey characteristics). The oldest photographs are black and white and are coloured since 1996. The photographs taken after 2000 were merged and orthorectified by IGN, but the merging and ortho-rectification process was required for earlier photographs. For a given survey date, all the photographs were assembled and merged using the photogrammetry software Agisoft Photoscan (v. 1.2.4). Here, Photoscan was used to build a 3D georeferenced model and further export of a full orthomosaic for each date.

A 4-step workflow was applied to georectify the photographs prior to 2000. (1) The alignment of each camera position was performed by detecting matching points on all overlapping couples of

Table 1
Characteristics of the aerial photo survey dataset from 1950 to 2014.

Date	Alongshore extent (km)	Areas	Pixel size (m)	Colour Data	Ground control points RMS error (m)
1950	296	(1), (2), (3), (4)	0.75 to 0.9	B&W	3.5 to 4.2
1964	130	(1), (2)	0.32 to 0.5	B&W	2.4
1965	70	(3), (4)	1	B&W	3.2 to 3.6
1973	240	(1), (2), (3)	0.5 to 0.9	B&W	1.4 to 3.6
1974	78	(4)	0.63	B&W	4.4
1984	240	(1), (2), (3)	0.5 to 0.9	B&W	2.3 to 5.6
1991	130	(1), (2)	0.43 to 0.5	B&W	3.7 to 3.9
1996	110	(3)	0.6	B&W	3.9
2000	110	(1)	0.5	Colour	3.6
2002	110	(4)	0.5	Colour	3.2
2006	20	(2)	0.5	Colour	Reference
2007	110	(4)	0.5	Colour	Reference
2009	110	(3)	0.5	Colour	Reference
2010	110	(1)	0.5	Colour	Reference
2014	360	(1), (2), (3), (4)	0.1 to 0.5	Colour	Reference

images. (2) A 3D dense cloud was built based on the camera alignment and was further used to generate a mesh. (3) The 3D model was georeferenced using salient fixed ground control points taken from the recent IGN referenced images (referred to as reference image in Table 1). These ground control points are fixed buildings, bridges and road intersections located approximately 500 m to 10 km from the shore with, on average, one ground control point every 2 km alongshore. A camera optimization procedure was performed to compute the intrinsic (lens distortion) and extrinsic (camera position) camera parameters by minimizing the error on the ground control points. (4) The dense cloud and the mesh were recomputed from the optimized camera positions allowing the generation of an accurate orthomosaic to be imported in a GIS software. The resulting orthomosaics were analysed with ArcMap GIS software (v. 10.3). The mean square error (RMSE) of each orthomosaic (Table 1) was computed at the ground control points using 2006, 2009 and 2010 images that were assumed as perfectly georeferenced.

3.2. Shoreline detection

The shoreline position was manually retrieved from each orthomosaic. It is well established that there is a large number of shoreline definitions (see the review of Boak and Turner, 2005). Given that long-term shoreline change of beach-dune systems from historical aerial photographs is addressed here, the dune foot and the limit of the vegetated foredune were defined as the shoreline position for eroding and accreting sectors, respectively (Fig. 3). This is consistent with previous shoreline change studies (e.g. Anderson et al., 2015; Fletcher et al., 2004; Kabuth et al., 2014). The shoreline was manually digitized by one operator. In order to estimate the errors in the shoreline position interpretation, two approaches were used. (1) Three other operators digitized the shoreline position on the oldest and poorest quality orthomosaic (1950) with, for instance, a substantial number of overexposed sectors where the dune and the beach were barely distinguishable. (2) The 2014 digitized shoreline position, which used the highest quality orthomosaic and is representative of image quality of the last 2 decades, was compared to the shoreline position measured in the field along the 110-km Gironde coast using a DGPS-equipped ATV (Fig. 4). For the latter, results show a bias of 0.4 m and a root mean square error of 1.8 m, meaning that the shoreline position from the aerial photograph is fairly accurate. Not surprisingly, results worsen for the 1950 shoreline for which a root mean square error and a bias of 12 m and 3 m were computed, respectively. However, given the magnitude of the shoreline evolution (see results) and the fact that

the 1950 orthomosaic is by far that of the worst quality, this first date of shoreline position was kept for the analysis.

3.3. Shoreline change analysis

Although efficient and user-friendly turnkey GIS tools exist for shoreline analysis (e.g. Thieler et al., 2017), here we developed our own shoreline analysis programs for flexibility. The digitized shorelines were all interpolated at a regular 0.2-m alongshore step. Inlet and estuary cross-sections, groins, dikes and jetties were all removed from the analysis. A low-pass filter was applied on each interpolated shoreline using a 2-km moving average window, in order to filter out local shoreline variability (e.g. beach entries) and rhythmic megacusp embayments cutting the dune during severe storms which have a typical wavelength of 400 m–1000 m along this coast (Castelle et al., 2015). Because it is both the most recent and more accurate shoreline dataset and because it covers the whole 270 km of coast, the filtered 2014 shoreline was chosen as the baseline. The orthogonal projection of each shoreline on the baseline was computed to obtain a cross-shore distance from the baseline and to further analyse shoreline change along the entire domain from $x = 0$ (Adour estuary) to $x = 280$ km in the north.

4. Results

4.1. Synoptic shoreline change

Fig. 5 shows the overall shoreline change since 1950 revealing a large temporal and alongshore variability of shoreline change over the last 64 years. Averaged over the 270 km of sandy coast, the shoreline retreated by 72 m within 64 years, that is, a spatially- and time-averaged erosion rate of 1.12 m/year. Although the overall erosion is 72 m, results also indicate more localized erosion hot-spots with shoreline erosion over 1950–2014 peaking at 700 m in the South of Oléron Island ($x = 275$ km in Fig. 5e), corresponding to an averaged erosion rate of approximately 11 m/year. More surprisingly, localized and scarce accreting sections of coast are observed. The most prominent accreting area is located immediately to the South of the Gironde estuary ($x = 234$ km, Fig. 5d) where the shoreline advanced by more than 450 m from 1950 to 2014. Overall, the largest shoreline variabilities are observed in the vicinity of the tidal inlets of Arcachon ($x = 125$ km) and Maumusson ($x = 272$ km), and in the vicinity of the Gironde estuary ($x = 250$ km). In contrast, the coastal towns with hard defence appear to have only a subtle impact on shoreline change at the nearby beaches. The only notable exception is Capbreton

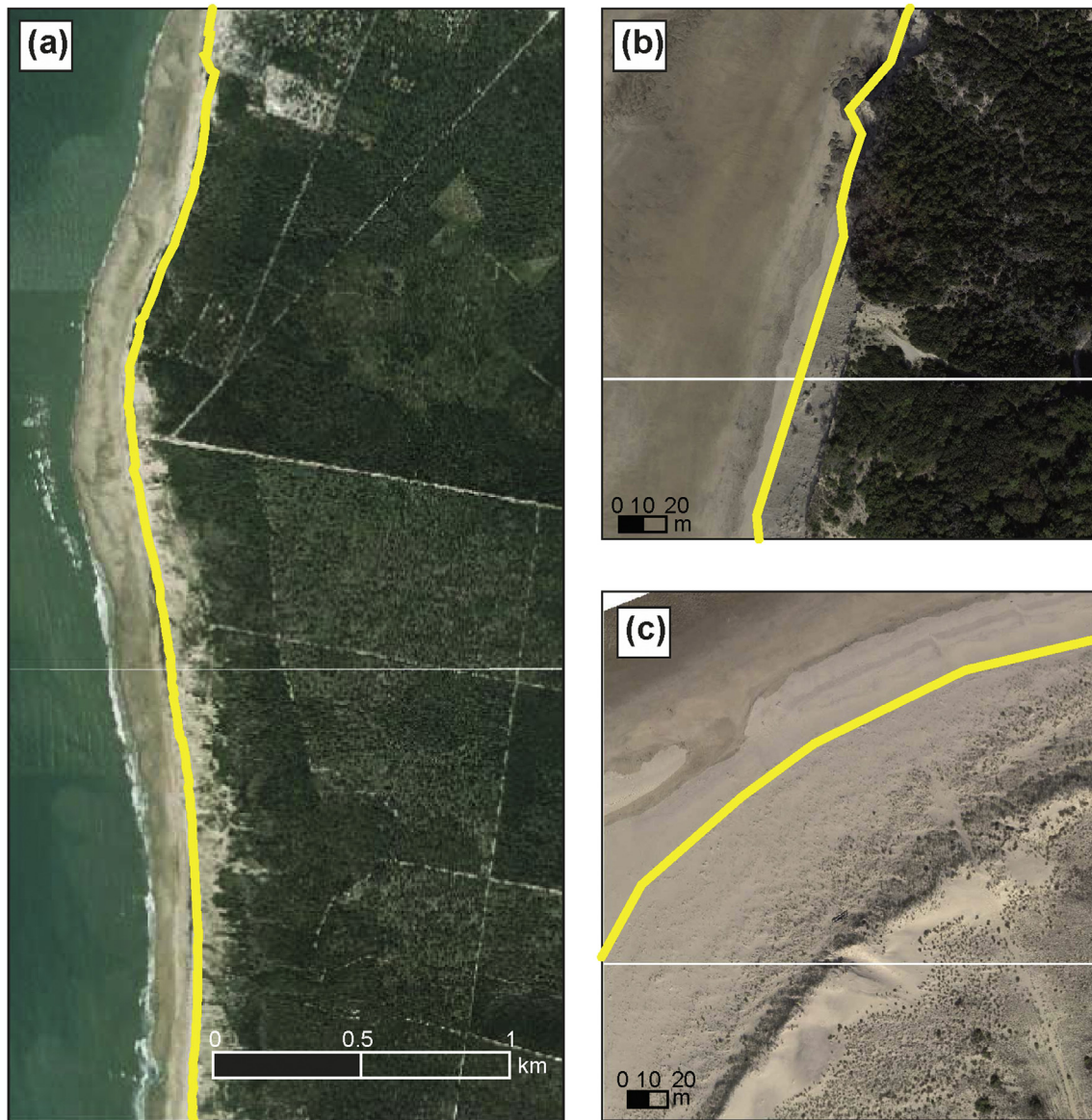


Fig. 3. Georeferenced photographs with superimposed shoreline position (yellow line) with (a) an overview field of the Pointe de la Négade; (b) a zoom onto a severely eroding sector where the shoreline is taken as the dune foot; (c) a zoom onto an accreting sector where the foredune vegetation limit is taken as the shoreline position. (For interpretation of the references to colour in this figure legend, the reader is referred to the web version of this article.)

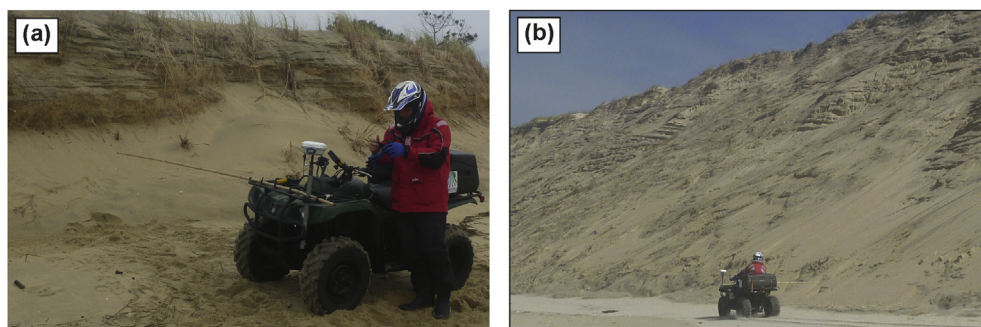


Fig. 4. The GPS-equipped ATV used to survey the shoreline in April 2014 along the 110-km Gironde coast (see Castelle et al., 2015), with (a) the 3-m stick to (b) drive approximately 2 m from the dune scarp to prevent from scarp collapse in severely eroding areas.

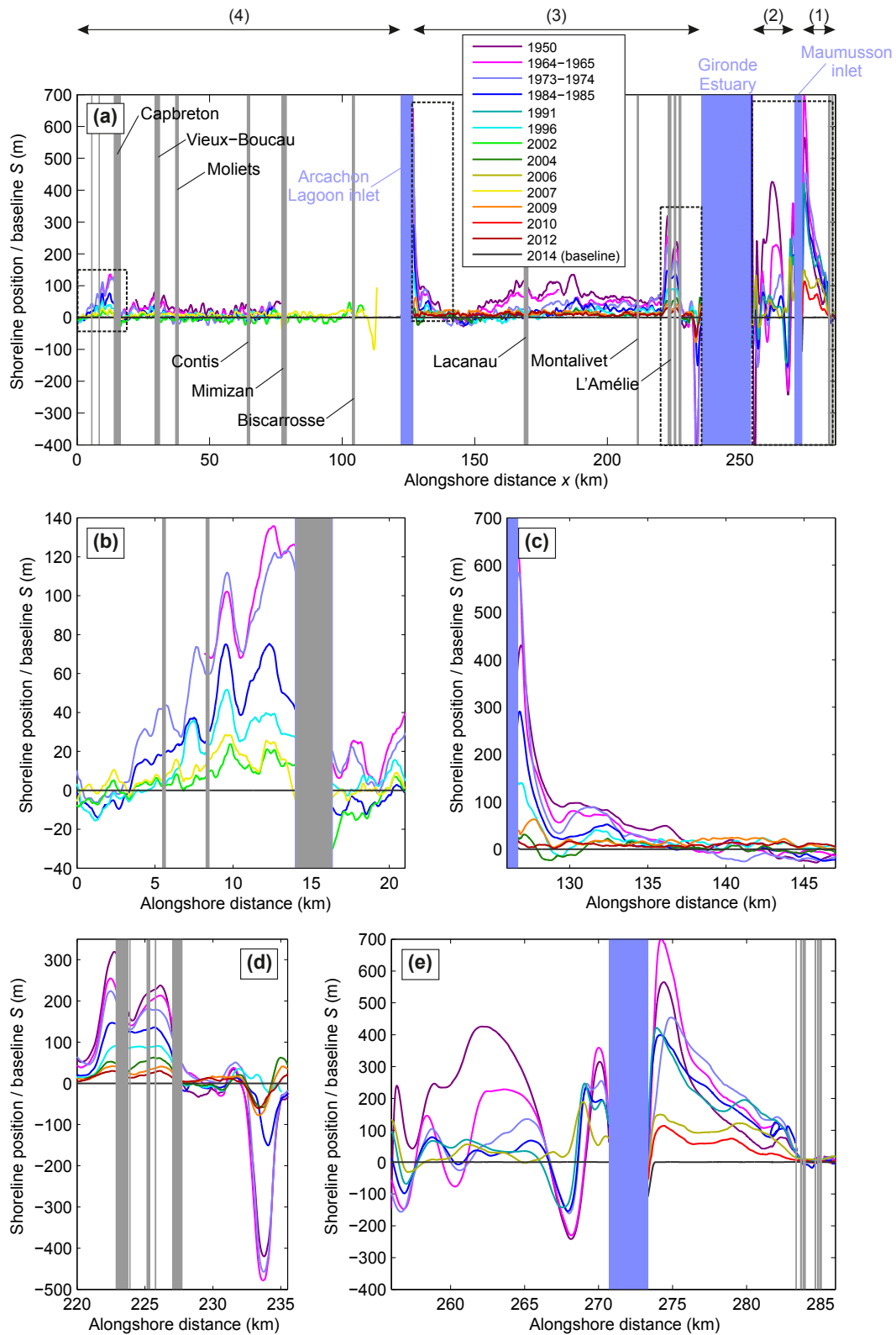


Fig. 5. (a) Time evolution of shoreline position S from south ($x = 0$) to north ($y = 270$ km) and from 1950 to 2014 with the dates coloured. Shoreline positions are all given with respect to the shoreline baseline defined in 2014, with positive S meaning that the shoreline is more seaward than in 2014. Coastal towns with hard defences as well as tidal inlets and estuaries interrupting the open coast are indicated by the vertical grey areas. Relevant coastal towns are also indicated. The four dashed black boxes indicate the zoomed areas provided in panels (b), (c), (d) and (e). (For interpretation of the references to colour in this figure legend, the reader is referred to the web version of this article.)

($x = 15$ km, Fig. 5b) where the southern downdrift beaches eroded by more than 100 m because of the northern jetty of the Capbreton harbour capturing most of the longshore drift. Another important pattern is the overall increasing erosion rate from south to north, with the presence of relatively stable sections such as in the south of the study area along most of the Landes coast ($40 \text{ km} < x < 100 \text{ km}$) and in the south of the Gironde coast ($140 \text{ km} < x < 150 \text{ km}$).

4.2. Time evolution of shoreline change

The temporal variability of shoreline position in relevant and representative locations are shown in Fig. 6. While substantial erosion is observed at most sites, contrasting temporal patterns of erosion can be depicted. (1) A quasi-steady erosion over the last 64 years, e.g. at the cape L'Amélie in the north of the Gironde coast where an average, reasonably constant, erosion rate of approximately 4.5 m/year is computed. (2) A 2-step evolution for which 3 different behaviours can be identified: (a) along the Arvert Peninsula, the shoreline retreated from the 1950s to the mid-1970s at a dramatic mean rate of approximately 15 m/year, before stabilizing from the mid-1970s onwards; (b) in the south of Oléron Island or at the tip of the Cap Ferret sandspit, a slow accretion from the 1950s to the mid-1970s (approximately +4 m/year) reversing into a dramatic erosion trend on the order of 10 m/year until now; (c) by opposition, in the northern sector of the Gironde coast at Pointe du Verdon, a slow erosion is observed from the 1950s to the mid-1970s (approximately -2 m/year), before a rapid accretion exceeding 20 m/year took place until the mid-1990s. (3) The last temporal pattern of shoreline change consists in a quasi-stable situation over the last 64 years, e.g. at the extensively studied Truc Vert beach located in the south of the Gironde coast. It is important to notice that these contrasting temporal patterns of shoreline change are part of a continuum, where more complex hybrid evolutions can be found.

4.3. Spatial patterns of shoreline change

It has been shown that shoreline change in SW France is strongly variable in both time and space. Below, we zoom from north to south onto relevant dynamic areas to give insight into the spatial and temporal shoreline evolution patterns. These dynamic areas often correspond to sectors adjacent to inlet and estuaries, or sectors that have been recently affected by coastal structures

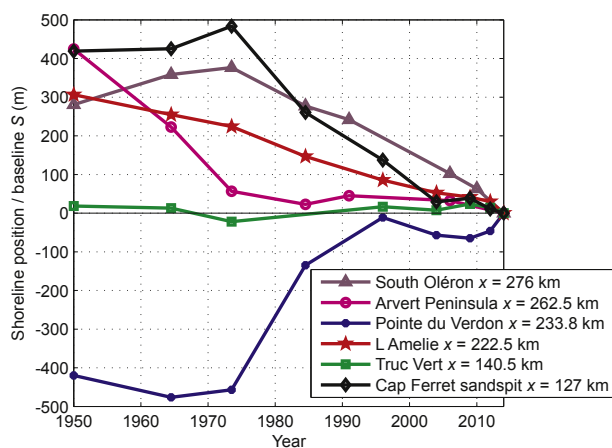


Fig. 6. Time evolution of shoreline position S at 6 representative locations in SW France. For all locations $S = 0$ is the shoreline position in 2014.

disrupting the alongshore sand transport pathways.

The sandy coast adjacent to the Maumusson inlet (Fig. 7) shows the largest spatial and temporal integrated shoreline variability of the entire study area (Fig. 5). The most striking pattern is found at the updrift coast with large and widespread erosion owing to the inward bending of the tip of the sandspit starting in the late 1970s, following a long period of overall accretion. The most erosive sector is located in the south of the area at $x = 274$ km with a notable acceleration in erosion rate that exceeded 17 m/year over the last 8 years (2006–2014). Erosion rates are less intense further north, e.g. at $x = 276$ km where the shoreline retreats at a rate of 5 m/year over the same period. This widespread erosion in the area since the 1970s resulted in the loss of 0.33 km^2 of land south of $x = 276$ km. Along this coast, the erosion was so rapid that the coastal dune system depleted to leave the coastal forest exposed to marine erosion at $275.5 \text{ km} < x < 273 \text{ km}$ since the early 2000s. Downdrift of the inlet ($x < 272$ m), shoreline change patterns are more complex with erosion and accretion alternating in both time and space, although overall erosion is found since 1950. The general erosion of the updrift and downdrift coast resulted in a widening of the inlet throat by approximately 500 m between 1950 and 2014.

Shoreline change south of the Gironde estuary can be discriminated into 3 areas (Fig. 8). (1) A relatively natural sector is observed at $234.3 \text{ km} < x < 236 \text{ km}$, which is essentially constrained by a jetty at the eastern end that was built in 1884 to minimize spit dynamics and resulting rapid shoreline changes. This sector has been relatively stable over time, although an overall slight accretion is observed, which recently reversed in the western part. (2) The sector at $232.5 \text{ km} < x < 234.3 \text{ km}$ showed a large accretion with the relatively straight section of coast reshaping into a rapidly accreting hook essentially between the 1960s and the 1980s. Overall, the land gained approximately 0.44 km^2 within only approximately 1.5 km of coast, with shoreline accretion reaching 550 m close to the centre of the shoreline bulge. The shoreline was subsequently quite stable over time, except in the eastern part where the land progressively gained approximately 0.1 km^2 , and in the western part where the shoreline advanced by approximately 50 m between 2010 and 2014 despite the high-energy winter of 2013/2014. Although this sector was trained with groins and breakwaters in the 19th century, all the structures were buried and did not impact shoreline change since

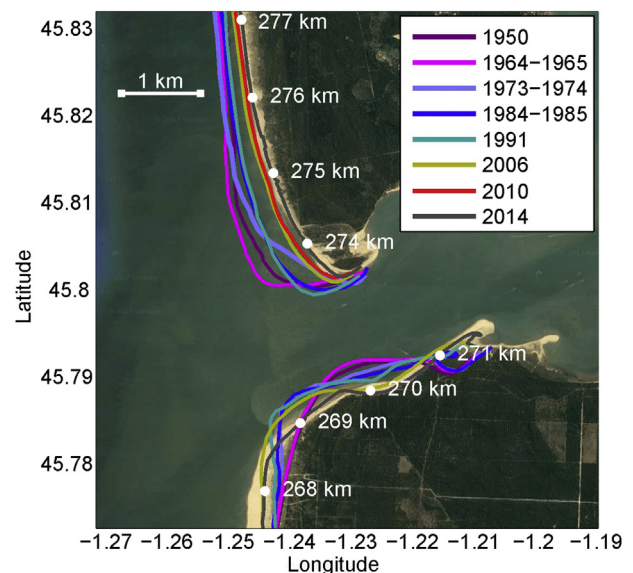


Fig. 7. Shoreline change between 1950 and 2014 along the coast adjacent to the Maumusson inlet.

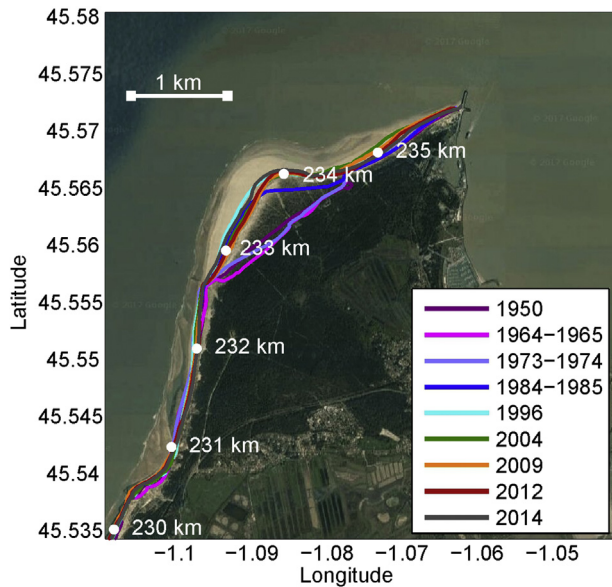


Fig. 8. Shoreline change between 1950 and 2014 along the coast south of the Gironde estuary.

1950. This sector is therefore quite preserved, with very limited beach access and with only one remaining groin at the southern end where shoreline orientation changes. (3) The sector south of $x = 232.5$ km has been stable. The sector $230.8 \text{ km} < x < 232.5$ km is relatively preserved, while the coast south of $x = 230.8$ km has been stable, essentially because it was trained with groins, jetties and breakwaters built in the 1920s in front of the coastal dune. These coastal works essentially fixed the shoreline preventing the dune system from wave attack.

The sector of Pointe de la Négade in the north of the Gironde coast has been under chronic, quasi-steady, erosion between 1950 and 2014 (Fig. 9), with high erosion rates despite this sector is more than 10 km away from the Gironde estuary mouth. The sector at $222 \text{ km} < x < 223 \text{ km}$ is largely impacted by an important linear erosion of 5 m/year from 1950 to 2014, peaking locally at 7.5 m/year between the 1970s and the 1990s, which represents a land loss of 0.3 km^2 in 64 years along 1 km of coast. Similar to the south of Oléron Island, the duration and severity of coastal erosion resulted in the depletion of the coastal dune system leaving the coastal forest directly exposed to marine erosion since the 1960s and the 1970s–1980 s at Amélie and Pointe de la Négade, respectively. Erosion rates decrease southwards where the coastal dune system is still present ($x < 222.2$ km), although erosion rates are quite severe (approximately 1.5 m/year). Another interesting shoreline change pattern is the stabilization of the shoreline since 2004 at $x > 223$ km due to the construction of a training wall to protect the small village of Amélie. The shoreline fixation was associated with a substantial increase in shoreline erosion in the south of the coastal structures exceeding 8 m/year between 2009 and 2014.

The Cap Ferret sandspit delimits the southern end of the Gironde coast (Fig. 10). The northern part ($128.5 \text{ km} < x < 130 \text{ km}$) has been slowly (0.7 m/year) eroding over the study period. Erosion at this sector is not too worrying as beaches are backed by high and wide (250–300 m) coastal dunes. Shoreline change at the tip of the sandspit further south is more complex and worrying with erosion rates dramatically increasing. After a rapid sandspit growth from the 1950s to the 1970 s at approximately 18 m/year, the sandspit underwent a substantial erosion from the 1970s to 2014 at a mean rate of 13 m/year. This corresponds to a retreat of 800 m at the tip and a land loss of approximately 0.75 km^2 of land south of

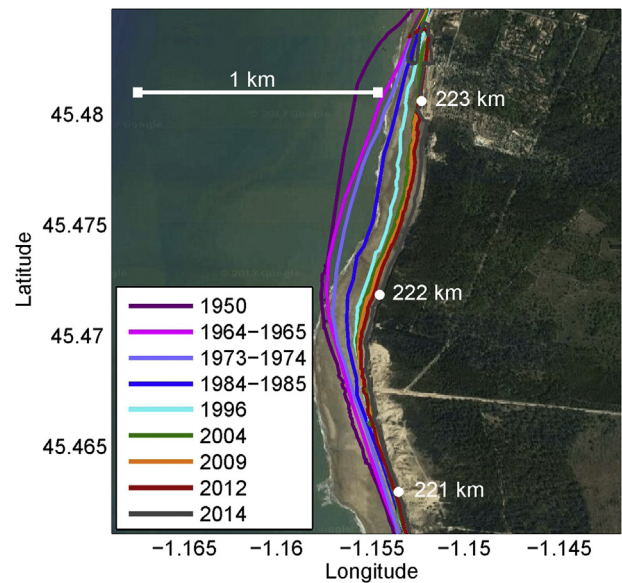


Fig. 9. Shoreline change between 1950 and 2014 along the Pointe de la Négade and Amélie in the north of the Gironde coast.

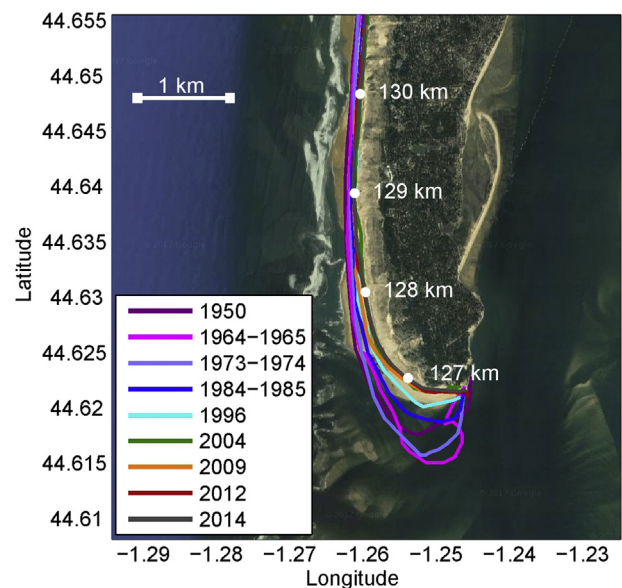


Fig. 10. Shoreline change between 1950 and 2014 at the Cap Ferret sandspit in the south of the Gironde coast.

$x = 128.5$ km. Interestingly enough, this 2-step sandspit evolution is synchronous to that of the Gatseau sandspit to the north of Mau-musson inlet, which will be discussed later in the paper.

5. Discussion

Over the 64-year study period, the high-energy 270-km sandy coast of SW France showed a profound temporal and spatial shoreline variability. Not only eroding, stable and accreting sectors alternate spatially, but they can also alternate over time with a substantial proportion of the coast (approximately 10%) experiencing a reverse in shoreline chronic change. These more complex sectors are essentially located close to the tidal inlets of Mau-musson and Arcachon and to the Gironde estuary mouth. At these

sectors, shoreline change is strongly impacted by the channel and shoal dynamics on long timescales, say decades. Obviously, the influence of a large-scale inlet such as that of Maumusson and Arcachon can impact long-term shoreline change of adjacent beaches more than 10 km away. Except locally where the shoreline has been fixed with coastal structures, the stable sectors are located well away from the inlets and estuary mouths. These stable regions are where alongshore gradients in longshore drift are negligible (Idier et al., 2013) owing to a straight nature of the open coast, which corresponds to most of the Landes coast and the southern part of the Gironde coast.

The Gatseau and Cap Ferret sandspits, which are located updrift of the 2 major tidal inlets, have been found to show a quasi-synchronous behaviour, despite the morphological expression of the two inlets is different (Cayocca, 2001; Bertin et al., 2005). This suggests that, instead of having a behaviour essentially controlled by an autocyclic mechanism as proposed by Bertin et al. (2004) for the Gatseau Spit, their dynamics may also be controlled by allocyclic mechanisms. Both inlets were found to show a shortening of the cross-section until the 1970s, corresponding to a rapid updrift sandspit growth and shoreline accretion. This trend dramatically reversed in the 1970s with a rapid sandspit retreat and shoreline erosion at the updrift coast. This erosion of the updrift coasts is still observed at the time of writing this paper. This is in line with Poirier et al. (2017) who showed that the shoreline dynamics at sand spits on both margins of the North Atlantic Ocean has been quasi-synchronous since approximately 1800 CE. The authors showed that natural modes of climate variability such as the North Atlantic Oscillation and East-Atlantic-West Russia atmospheric circulation pattern only partially explain this evolution. Therefore, at this stage it is not possible to conclude if this is due to a change in the longshore drift component since the 1970s or if, because of sea level rise, the increase in tidal prism is responsible for the increase in inlet cross-section. The role of the decrease in river sediment supply, which was found of great importance in other environments (e.g. Anthony, 2014; Roszkopf et al., 2017) should also be quantified. This will need to be explored through numerical modelling, with more comparison with other beaches adjacent to large-scale tidal inlets further south as our study shows that the synchronous change not only affects the shoreline at the sandpit but also further along the more updrift coast.

Averaged over the period 1950–2014, the south of Oléron Island (1.83 m/year) and the Arvert coast (2.78 m/year) are the most eroding sectors, with lowest erosion rates for the Gironde (0.94 m/year) and Landes (0.41 m/year between Capbreton and Mimizan) coasts. The mean shoreline change computed over the 4 sectors above indicate a temporally and spatially averaged shoreline erosion rate of 1.12 m/year. Interestingly, there was no significant increase in the spatially averaged erosion rate in the recent decades (see Fig. 11), although the different sectors locally show different behaviours. This is counter-intuitive given the well-established increase in sea-level-rise rate in W France over the last decades. Increasing erosion rates were also expected because of the subtle increase in winter wave height (e.g. Bertin et al., 2013) and the recent outstanding winter of 2013–2014, which caused large-scale erosion in SW France (Castelle et al., 2015). In addition, using the average beach profile characteristics of the SW France beaches the Bruun effect gives a sea-level-rise-driven erosion an order of magnitude smaller than that observed on average between 1950 and 2014. Sea-level-rise driven inlet-estuary/lagoon infilling can drive increased erosion on the sectors adjacent to the Gironde estuary and Maumusson and Arcachon inlets (Stive and Wang, 2003; Ranasinghe et al., 2013), although unlikely up to an order of magnitude. This suggests that other parameters control the chronic erosion at these temporal scales (Le Cozannet et al., 2016), with the

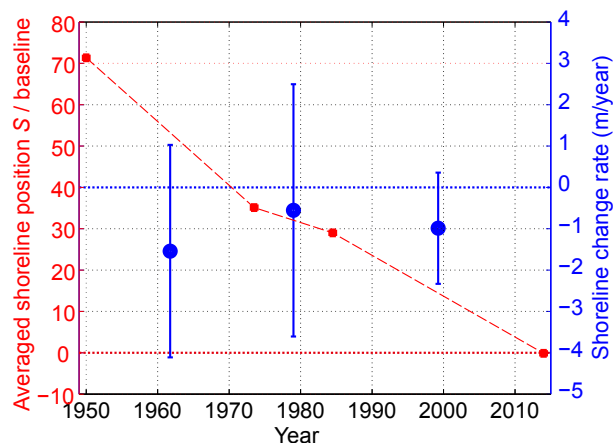


Fig. 11. Alongshore-averaged shoreline position S (red) and resulting erosion rate (blue) computed over the sectors (1), (2) and (3) indicated in Fig. 1. (For interpretation of the references to colour in this figure legend, the reader is referred to the web version of this article.)

deficit in sediment input from the inner shelf being the most plausible (Prat and Salomon, 1997).

The fact that there has been no increase in erosion rate since the 1980s may be caused by the coastal dune management by the French National Forest Office (ONF). The coastal dune system was established in the nineteenth century when gourbet and oyat (*Ammophila arenaria*) were extensively planted. However the coastal dune suffered severe damages from some outstanding winter storms in the 1910s and 1920s and the Second World War during which the coastal dunes were restricted areas used as a source of aggregate to build the Nazi blockhouses. Until the early 1960s, the coastal dunes were in serious disrepair, being eroded by the sea, dissected by blowouts and hollowed out as gullies. The ONF undertook extensive renovation between the 1960s and the 1980s using large-scale mechanical aid. Over these 2–3 decades the extensive dune profiling and marran planting resulted in a systematic shoreline retreat as a result of natural adjustment of the dune profile from the engineered profile (Barrère, 1992). As a result, the lack of significant increase in erosion rate over the last decades can be due to abnormal high erosion rate prior to the 1980s owing to the total disrepair of the coastal dunes in the 1940s and 1950s and the subsequent profiling until the early 1980s. In other words, the coastal dune management performed by the ONF may have strongly limited natural erosion over the last 3 decades. This overall erosion trend will need to be explored further using more accurate and higher frequency shoreline data in the next decades and linking up with wave conditions.

This 270-km coast studied here is relatively preserved from human intervention. Most of the rare coastal structures are found to impact shoreline dynamics locally through shoreline fixing. The impact further along the coast is variable depending mostly on how far the coastal structures extend offshore. An example (not shown) of a shoreline behaviour in line with what is commonly documented in the literature is the coastal town of Capbreton where groins and training wall captured the southerly longshore drift result in the rapid erosion of the downdrift coast (see at $x = 15$ km in Fig. 5b), which forced the recent implementation of a bypassing system. Other coastal structures have a more localized impact such as south of Soulac at Amélie (Fig. 9). More surprisingly, the influence of the coastal towns built on the dune (Fig. 2b) such as Montalivet, Lacanau and Mimizan which are all protected by an alongshore training wall and a couple of short-scale groins not extending further the intertidal domain, have a negligible impact so

far. No significant difference in shoreline change was observed between the updrift and downdrift coasts of these towns. However, the training walls have only been recently located further offshore of the natural shoreline and exposed to wave attack after the winter 2013/2014. Therefore, the impact of the coastal towns on the nearby beaches may become increasingly visible as the shoreline further erodes and expose the training wall disrupting the long-shore drift.

6. Conclusions

This study shows that shoreline change along a high-energy sandy coast disrupted by two large-scale tidal inlets, an estuary mouth and a few coastal towns exhibits large spatial and temporal variability. The coasts adjacent to the inlets and the estuary mouth are the most dynamic with erosion and accretion alternating over time on the scale of decades, which can be captured if shoreline data collected at least every 10 years is used. The inlet-sandspit systems show a striking quasi-synchronous behaviour suggesting that the large-scale dynamics of the nearby coast is controlled by allocyclic mechanisms in addition to autocyclic mechanisms, although the primary mechanism must be explored further. An overall erosion trend is found when averaging spatially the data, which is not essentially caused by sea level rise. This trend has been rather steady over the last 64 years, with the dune restoration and management strategy being hypothesized to have limited the coastal erosion over the last decades. Overall, this study suggests that long-term shoreline change of high-energy sandy coasts disrupted by inlets and/or estuaries is complex and needs to consider a wide range of parameters including, non-extensively, waves, tides, inlet dynamics, sea level rise, coastal dune management and coastal defences. This challenges the development of numerical models encompassing all these processes, which eventually will provide fair estimate of the respective contribution of all these processes on the observed evolution.

Acknowledgments

This work was done within the framework of project CHIPO (ANR-14-ASTR-0004) and SONO (ANR-17-CE01-0014) funded through the Agence Nationale de la Recherche (ANR). This study covers a number of monitoring study sites of the Service National d'Observation (SNO) Dynalit labelled by CNRS-INSU which, together with the Observatoire de la Côte Aquitaine (OCA), provide financial support to survey the coast. We thank MCIA for providing data storage facilities for this study. Some of the data presented here was collected as part of a complementary PhD work of BG with the District of Oléron Island.

References

Abadie, S., Butel, R., Mauriet, S., Morichon, D., Dupuis, H., 2006. Wave climate and longshore drift on the South Aquitaine coast. *Cont. Shelf Res.* 26, 1924–1939.

Allard, J., Chaumillon, E., Bertin, X., Poirier, C., Ganthy, F., 2010. Secular morphological evolution and Holocene stratigraphy of a macro tidal bay: the Marennes-Oléron Bay (SW France). In: Chaumillon, E., Tessier, B., Reynaud, J.-Y. (Eds.), *French Incised Valleys and estuaries*, Bulletin de la Société géologique de France, numéro thématique, pp. 151–169 t. 181, n°2.

Almonacid-Caballer, J., Sánchez-García, E., Pardo-Pascual, J.E., Balaguer-Beser, A.A., Palomar-Vázquez, J., 2016. Evaluation of annual mean shoreline position deduced from Landsat imagery as a mid-term coastal evolution indicator. *Mar. Geol.* 372, 79–88. <https://doi.org/10.1016/j.margeo.2015.12.015>.

Anderson, T.R., Frazer, L.N., Fletcher, C.H., 2015. Long-term shoreline change at kailua, Hawaii, using regularized single transect. *J. Coast. Res.* 300, 464–476. <https://doi.org/10.2112/JCOASTRES-D-13-00202.1>.

Anthony, E.J., 2014. The Human influence on the Mediterranean coast over the last 200 years: a brief appraisal from a geomorphological perspective. *Geomorphologie relief, Process. Environ.* 20, 219–226.

Barrère, P., 1992. Dynamics and management of the coastal dunes of the Landes,

Gascony, France. In: Carter, R.W.G., et al. (Eds.), *Coastal Dunes: Geomorphology, Ecology and Management for Conservation: Proceedings of the 3rd European Dune Congress*, Galway, Ireland, pp. 25–32.

Baumann, J., Chaumillon, E., Bertin, X., Schneider, J.-L., Guillot, B., Schmutz, M., 2017. Importance of infragravity waves for the generation of washover deposits. *Mar. Geol.* 391, 20–35.

Bertin, X., Chaumillon, E., Weber, N., Tesson, M., 2004. Morphological evolution and coupling with bedrock within a mixed energy tidal inlet: the Maumusson Inlet, Bay of Biscay, France. *Mar. Geol.* 204, 187–202.

Bertin, X., Chaumillon, E., Sottolichio, A., Pedreros, R., 2005. Tidal inlet response to sediment infilling of the associated bay and possible implications of human activities: the Marennes-Oléron Bay and the Maumusson Inlet, France. *Cont. Shelf Res.* 25, 1115–1131. <https://doi.org/10.1016/j.csr.2004.12.004>.

Bertin, X., Castelle, B., Chaumillon, E., Butel, R., Quique, R., 2008. Longshore drift estimation and inter-annual variability at a high-energy dissipative beach: st. Trojan Beach, SW Oléron Island, France. *Cont. Shelf Res.* 28, 1316–1332.

Bertin, X., Prouteau, E., Letetrel, C., 2013. A significant increase in wave height in the North Atlantic of the 20th century. *Glob. Planet. Change* 106, 77–83.

Boak, E.H., Turner, I.L., 2005. Shoreline definition and detection: a review. *J. Coast. Res.* 21 (4), 688–703.

Bouvier, C., Balouin, Y., Castelle, B., 2017. Video monitoring of sandbar-shoreline response to an offshore submerged structure at a microtidal beach. *Geomorphology* 295, 297–305.

Bruun, P., 1962. Sea-level Rise as a Cause of Shore Erosion. Florida Engineering and Industrial Experiment Station.

Butel, R., Dupuis, H., Bonneton, P., 2002. Spatial variability of wave conditions on the French Atlantic coast using in-situ data. *J. Coast. Res.* 36, 96–108.

Castelle, B., Bourget, J., Molnar, N., Strauss, D., Deschamps, S., Tomlinson, R., 2007. Dynamics of a wave-dominated tidal inlet and influence on adjacent beaches, Currumbin Creek, Gold Coast, Australia. *Coast. Eng.* 54, 77–90. <https://doi.org/10.1016/j.coastaleng.2006.08.007>.

Castelle, B., Bujan, S., Ferreira, S., Dodet, G., 2017a. Foredune morphological changes and beach recovery from the extreme 2013/2014 winter at a high-energy sandy coast. *Mar. Geol.* 385, 41–55. <https://doi.org/10.1016/j.margeo.2016.12.006>.

Castelle, B., Dodet, G., Masselink, G., Scott, T., 2017b. A new climate index controlling winter wave activity along the atlantic coast of Europe: the West Europe pressure anomaly: West Europe pressure anomaly. *Geophys. Res. Lett.* 44, 1384–1392. <https://doi.org/10.1002/2016GL072379>.

Castelle, B., Marieu, V., Bujan, S., Splinter, K.D., Robinet, A., Sénéchal, N., Ferreira, S., 2015. Impact of the winter 2013–2014 series of severe Western Europe storms on a double-barred sandy coast: beach and dune erosion and megacusp embayments. *Geomorphology* 238, 135–148. <https://doi.org/10.1016/j.geomorph.2015.03.006>.

Cayocca, F., 2001. Long-term morphological modeling of a tidal inlet: the Arcachon Basin, France. *Coast. Eng.* 42, 115–142. [https://doi.org/10.1016/S0378-3839\(00\)00053-3](https://doi.org/10.1016/S0378-3839(00)00053-3).

Cazenave, A., Dieng, H.-B., Meyssignac, B., von Schuckmann, K., Decharme, B., Berthier, E., 2014. The rate of sea-level rise. *Nat. Clim. Change* 4, 358–361. <https://doi.org/10.1038/nclimate2159>.

Chaaban, F., Darwishe, H., Battiau-Queney, Y., Louche, B., Masson, E., Khattabi, J.E., Carlier, E., 2012. Using ArcGIS® modelbuilder and aerial photographs to measure coastline retreat and advance: north of France. *J. Coast. Res.* 285, 1567–1579. <https://doi.org/10.2112/JCOASTRES-D-11-00054.1>.

Chaumillon, E., Proust, J.-N., Menier, D., Weber, N., 2008. Incised-valley morphologies and sedimentary-fills within the inner shelf of the Bay of Biscay (France): a synthesis. *J. Mar. Syst.* 72, 383–396.

Cohen, J.E., 1997. Estimates of coastal populations. *Science* 278, 1209c–1213. <https://doi.org/10.1126/science.278.5341.1209c>.

Cooper, J.A.G., Pilkey, O.H., 2004. Sea-level rise and shoreline retreat: time to abandon the Bruun Rule. *Glob. Planet. Change* 43, 157–171. <https://doi.org/10.1016/j.gloplacha.2004.07.001>.

Davidson, M.A., Splinter, K.D., Turner, I.L., 2013. A simple equilibrium model for predicting shoreline change. *Coast. Eng.* 73, 191–202. <https://doi.org/10.1016/j.coastaleng.2012.11.002>.

Dodet, G., Bertin, X., Taborda, R., 2010. Wave climate variability in the North-East Atlantic Ocean over the last six decades. *Ocean. Model.* 31, 120–131. <https://doi.org/10.1016/j.ocemod.2009.10.010>.

Féniès, H., Lericolais, G., Posamentier, H.W., 2010. Comparison of wave- and tide-dominated incised valleys: specific processes controlling systems tract architecture and reservoir geometry. *Bull. Société géologique Fr.* 181 (2), 171–181. <https://doi.org/10.2113/gssgfbull.181.2.171>.

Firth, L.B., Thompson, R.C., Bohn, K., Abbiati, M., Airoldi, L., Bouma, T.J., Bozzeda, F., Ceccherelli, V.U., Colangelo, M.A., Evans, A., Ferrario, F., Hanley, M.E., Hinz, H., Hoggart, S.P.G., Jackson, J.E., Moore, P., Morgan, E.H., Perkol-Finkel, S., Skov, M.W., Strain, E.M., van Belzen, J., Hawkins, S.J., 2014. Between a rock and a hard place: environmental and engineering considerations when designing coastal defence structures. *Coast. Eng.* 87, 122–135.

Fletcher, C., Rooney, J., Barbee, M., Lim, S.-C., Richmond, B., 2004. Mapping shoreline change using digital orthophotogrammetry on maui, Hawaii. *J. Coast. Res.* 106–124.

Ford, M., 2013. Shoreline changes interpreted from multi-temporal aerial photographs and high resolution satellite images: wotje Atoll, Marshall Islands. *Remote Sens. Environ.* 135, 130–140. <https://doi.org/10.1016/j.rse.2013.03.027>.

Ghermandi, A., Nunes, P.A.L.D.n., 2013. A global map of coastal recreation values: results from a spatially explicit meta-analysis. *Ecol. Econ.* 86, 1–15.

- Grunnet, N.M., Ruessink, B.G., 2005. Morphodynamic response of nearshore bars to a shoreface nourishment. *Coast. Eng.* 52, 119–137. <https://doi.org/10.1016/j.coastaleng.2004.09.006>.
- Idier, D., Castelle, B., Charles, E., Mallet, C., 2013. Longshore sediment flux hindcast: spatio-temporal variability along the SW Atlantic coast of France. *J. Coast. Res.* 165, 1785–1790. <https://doi.org/10.2112/S165-302.1>.
- Kabuth, A.K., Kroon, A., Pedersen, J.B.T., 2014. Multidecadal shoreline changes in Denmark. *J. Coast. Res.* 296, 714–728. <https://doi.org/10.2112/JCOASTRES-D-13-00139.1>.
- Klingebl, A., Gayet, J., 1995. Fluvio-lagoonal sedimentary sequences in Leyre delta and Arcachon bay, and Holocene sea level variations, along the Aquitaine coast (France). *Quat. Int.* 29–30, 111–117.
- Le Cann, B., 1990. Barotropic tidal dynamics of the Bay of Biscay shelf: observations, numerical modelling and physical interpretation. *Cont. Shelf Res.* 10, 723–758. [https://doi.org/10.1016/0278-4343\(90\)90008-A](https://doi.org/10.1016/0278-4343(90)90008-A).
- Le Cozannet, G., Oliveros, C., Castelle, B., Garcin, M., Idier, D., Pedreros, R., Rohmer, J., 2016. Uncertainties in sandy shorelines evolution under the Bruun rule assumption. *Front. Mar. Sci.* 3 <https://doi.org/10.3389/fmars.2016.00049>.
- List, J.H., Sallenger, A.H., Hansen, M.E., Jaffe, B.E., 1997. Accelerated relative sea-level rise and rapid coastal erosion. *Mar. Geol.* 140, 347–365. [https://doi.org/10.1016/S0025-3227\(97\)00035-2](https://doi.org/10.1016/S0025-3227(97)00035-2).
- Martínez, M.L., Hesp, P.A., Gallego-Fernández, J.B., 2013. Coastal dunes: human impact and need for restoration. In: Martínez, M.L., Gallego-Fernández, J.B., Hesp, P.A. (Eds.), *Restoration of Coastal Dunes*. Springer Berlin Heidelberg, Berlin, Heidelberg, pp. 1–14. https://doi.org/10.1007/978-3-642-33445-0_1.
- Masselink, G., Castelle, B., Scott, T., Dodet, G., Suanez, S., Jackson, D., Floc'h, F., 2016. Extreme wave activity during 2013/2014 winter and morphological impacts along the Atlantic coast of Europe. *Geophys. Res. Lett.* 43, 2135–2143. <https://doi.org/10.1002/2015GL067492>.
- Mazieres, A., Gillet, H., Castelle, B., Mulder, T., Guyot, C., Garlan, T., Mallet, C., 2014. High-resolution morphobathymetric analysis and evolution of Capbreton submarine canyon head (Southeast Bay of Biscay - French Atlantic Coast) over the last decade using descriptive and numerical modeling. *Mar. Geol.* 351, 1–12.
- Nienhuis, J.H., Ashton, A.D., Nardin, W., Fagherazzi, S., Giosan, L., 2016. Alongshore sediment bypassing as a control on river mouth morphodynamics: LITTORAL BYPASSING. *J. Geophys. Res. Earth Surf.* 121, 664–683. <https://doi.org/10.1002/2015JF003780>.
- Prat, M.C., Salomon, J.N., 1997. The recent evolution of the Charente coast. *Shorelines and dune systems*. *Quaternaire* 8, 21–37.
- Poirier, C., Tessier, B., Chaumillon, E., Bertin, X., Fruergaard, M., Mouazé, D., Noël, S., Weill, P., Wöppelmann, G., 2017. Decadal changes in North Atlantic atmospheric circulation patterns recorded by sand spits since 1800 CE. *Geomorphology* 281, 1–12.
- Pranzini, E., Williams, A.T., 2013. *Coastal Erosion and Protection in Europe*. Routledge, Abingdon, p. 488.
- Ranasinghe, R., Turner, I.L., 2006. Shoreline response to submerged structures: a review. *Coast. Eng.* 53, 65–79.
- Ranasinghe, R., Duong, T.M., Uhlenbrook, S., Roelvink, J.A., Stive, M.J.H.F., 2013. Climate Change impact assessment for inlet-in interrupted coastlines. *Nat. Clim. Change* 3, 83–87.
- Regnaud, H., Jennings, S., Delaney, C., Lemasson, L., 1996. Holocene sea-level variations and geomorphological response: an example from northern Brittany (France). *Quat. Sci. Rev.* 15, 781–787. [https://doi.org/10.1016/S0277-3791\(96\)00070-4](https://doi.org/10.1016/S0277-3791(96)00070-4).
- Ridderinkhof, W., Hoekstra, P., van der Vegt, M., de Swart, H.E., 2016. Cyclic behavior of sandy shoals on the ebb-tidal deltas of the Wadden Sea. *Cont. Shelf Res.* 115, 14–26. <https://doi.org/10.1016/j.csr.2015.12.014>.
- Robinet, A., Castelle, B., Idier, D., Le Cozannet, G., Déqué, M., Charles, E., 2016. Statistical modeling of interannual shoreline change driven by North Atlantic climate variability spanning 2000–2014 in the Bay of Biscay. *Geo-Mar. Lett.* 36, 479–490. <https://doi.org/10.1007/s00367-016-0460-8>.
- Rosati, J.D., 2005. Concepts in sediment budgets. *J. Coast. Res.* 212, 307–322. <https://doi.org/10.2112/02-475A.1>.
- Roskopf, C.M., Di Paola, G., Atkinson, D.E., et al., 2017. Recent shoreline evolution and beach erosion along the central Adriatic coast of Italy: the case of Molise region. *J. Coast. Conserv.* <https://doi.org/10.1007/s11852-017-0550-4>.
- Scott, T., Masselink, G., O'Hare, T., Saulter, A., Poate, T., Russell, P., Davidson, M., Conley, D., 2016. The extreme 2013/2014 winter storms: beach recovery along the southwest coast of England. *Mar. Geol.* 382, 224–241. <https://doi.org/10.1016/j.margeo.2016.10.011>.
- Splinter, K.D., Turner, I.L., Davidson, M.A., Barnard, P., Castelle, B., Oltman-Shay, J., 2014. A generalized equilibrium model for predicting daily to interannual shoreline response. *J. Geophys. Res.* 119, 1936–1958. <https://doi.org/10.1002/2014JF003106>.
- Stive, M.J., Aarninkhof, S.G., Hamm, L., Hanson, H., Larson, M., Wijnberg, K.M., Nicholls, R.J., Capobianco, M., 2002. Variability of shore and shoreline evolution. *Coast. Eng.* 47, 211–235. [https://doi.org/10.1016/S0378-3839\(02\)00126-6](https://doi.org/10.1016/S0378-3839(02)00126-6).
- Stive, M.J.F., Wang, Z.B., 2003. Morphodynamic modeling of tidal basins and coastal inlets. In: Lakhani, C. (Ed.), *Advances in Coastal Modeling*. Elsevier, pp. 367–392.
- Thieler, E.R., Himmelstoss, E.A., Zichichi, J.L., Ergul, A., 2017. Digital Shoreline Analysis System (DSAS) Version 4.0—An ArcGIS Extension for Calculating Shoreline Change (Ver. 4.4, July 2017): U.S. Geological Survey Open-file Report 2008–1278. <https://pubs.er.usgs.gov/publication/ofr20081278>.
- Turner, I.L., Harley, M.D., Short, A.D., Simmons, J.A., Bracs, M.A., Phillips, M.S., Splinter, K.D., 2016. A multi-decade dataset of monthly beach profile surveys and inshore wave forcing at Narrabeen. *Aust. Sci. Data* 3, 160024. <https://doi.org/10.1038/sdata.2016.24>.
- Vellinga, P., Leatherman, S.P., 1989. Sea level rise, consequences and policies. *Clim. Change* 15 (1–2), 175–189. <https://doi.org/10.1007/bf00138851>.
- Weggel, J.R., 1979. A Method for Estimating Long-term Erosion Rates from a Long-term Rise in Water Level. Coastal engineering technical aid;79-2. U.S. Army Coastal Engineering Research Center; National Technical Information Service, Operations Division, Fort Belvoir, Virginia, Springfield, Virginia.
- Weidman, C.R., Ebert, J.R., 1993. Cyclic spit morphology in a developing inlet system. In: Aubrey, D.G., Giese, G.S. (Eds.), *Formation and Evolution of Multiple Tidal Inlet Systems*, vol. 44. American Geophysical Union, Washington D.C., pp. 158–185.
- Yates, M.L., Guza, R.T., O'Reilly, W.C., 2009. Equilibrium shoreline response: observations and modeling. *J. Geophys. Res.* 114 <https://doi.org/10.1029/2009JC005359>.
- Zappa, G., Shaffrey, L.C., Hodges, K.I., Sansom, P.G., Stephenson, D.B., 2013. A multimodel assessment of future projections of North Atlantic and European extratropical cyclones in the CMIP5 climate models. *J. Clim.* 26, 5846–5862. <https://doi.org/10.1175/JCLI-D-12-00573>.